Original Article

Iranian Journal of Immunology

December 2025; 22(4):310-321.

Antitumor Effects of Tumor-Derived Exosomes in Murine Hepatocellular Carcinoma Models

Weibing Xu[1], Lulu Fan[2*]

[1]Center for Scientific Research of the First Affiliated Hospital of Anhui Medical University, 218 Jixi Road, Hefei, Anhui Province 230022, China; [2]Department of Oncology, The First Affiliated Hospital of Anhui Medical University, 218 Jixi Road, Hefei, Anhui Province 230022, China

ABSTRACT

Background: Exosomes (EXOs) are small vesicles derived from endosomes and secreted by most living cells including tumor cells. In recent years, these vesicles have been recognized as key mediators of intercellular communication, playing essential roles in the regulation and orchestration of diverse physiological and pathological processes within the organism.

Objective: To further investigate hepatocellular carcinoma (HCC)-derived exosomes containing tumor-associated antigens and to evaluate their immunostimulatory capacity and antitumor effects using *in vitro* and *in vivo* approaches.

Methods: Following isolation from tumor cells, exosomes were characterized and subsequently co-cultured with dendritic cells (DCs). The expression of surface molecules associated with DC maturation was then assessed using flow cytometry. A mouse liver cancer model was established and animals were randomly assigned to three groups: a negative control group (treated with PBS), an iDC group, and a DC-TEXs (tumor-derived exosomes) group. Tumor volume was monitored in all groups, with a focus on changes in immune cell populations and cytokine levels.

Results: Our *in vitro* studies showed that Hepa1-6 cell-derived EXOs dose-dependently enhanced dendritic cell (DC) maturation, as evidenced by increased expression of surface MHC-II molecules, co-stimulatory markers (CD40, CD80, CD86), and the maturation marker CD83. In vivo studies using subcutaneous HCC mouse models demonstrated that TEX administration significantly alters the tumor immune microenvironment, mainly through increased T lymphocyte infiltration and proliferation.

Conclusion: Our results suggest that TEXs can serve as endogenous immunotherapeutic agents by eliciting tumor-specific T lymphocyte responses through DC activation cascades. These findings provide novel insights into the therapeutic exploitation of tumor-derived vesicles for the treatment of hepatocellular carcinoma.

Keywords: Dendritic cell, Exosomes, Hepatocellular Carcinoma, Immunotherapy

*Corresponding author:
Lulu Fan,
Department of Oncology, The First Affiliated Hospital of Anhui Medical University, 218 Jixi Road, Hefei, Anhui Province 230022, China
Email: fanlulu8332@sina.com

Cite this article as:
Xu W, Fan L. Antitumor Effects of Tumor-Derived Exosomes in Murine Hepatocellular Carcinoma Models. *Iran J Immunol.* 2025; 22(4): 310-321, doi: 10.22034/iji.2025.106436.3025.

Received: 2025-04-25
Revised: 2025-08-06
Accepted: 2025-09-03

INTRODUCTION

Hepatocellular carcinoma (HCC) remains a significant global health challenge (1, 2). Currently, surgery is the primary treatment for HCC. However, HCC is often diagnosed at intermediate or advanced stages, necessitating comprehensive treatments such as interventional therapy, radiochemotherapy and drug targeted therapy. The curative effect of these treatments is not always satisfactory (3-5). In recent years, immunotherapy has emerged as a promising breakthrough in the treatment of HCC, with dendritic cell-based immunotherapy representing a cutting-edge area of research (6-8).

Recently, the physiological role of EXOs has sparked the interest of tumor researchers (9, 10). EXOs are small vesicles ranging in size from approximately 30 to 120 nm in diameter (11), which are widely present in various body secretions, such as cerebrospinal fluid, urine, blood, saliva, etc.(12-15). Exosomes, derived from endosomal compartments (multivesicular bodies), can reflect many of the biological characteristics of parental cells (16, 17). They mediate immune responses through multiple mechanisms. Exosomes derived from antigen-presenting cells act as carriers of MHC class I/II-peptide complexes, allowing them to directly activate CD8+ or CD4+ T cells, while exosomal HSP70 enhances dendritic cell maturation by binding to TLR2/4. Through cargo transfer, exosomes deliver immunomodulatory molecules that regulate immune cell function. Notably tumor-derived exosomal PD-L1 suppresses T-cell activity by engaging with PD-1. Furthermore, exosomes facilitate intercellular communication by transferring cytokines (e.g., IL-10, TNF-α) and metabolites, which can influence macrophage polarization and collectively shape immune responses through integrated signaling pathways. In contrast, $CD8^+$ T lymphocytes directly eliminate tumor cells by recognizing tumor antigens presented via MHC class I molecules. Therefore, whether TEXs can carry tumor-specific antigens and induce a $CD8^+$ T lymphocyte–dependent, tumor-specific immune response through uptake, processing and antigen presentation by antigen-presenting cells (APCs) remains to be further elucidated.

Here, we investigated the function and feasibility of using exosomes derived from Hepa 1-6 cell to stimulate immune response in a mouse model of HCC. We demonstrated that Hepa 1-6–derived exosomes induced a robust antitumor immune response by transferring tumor antigens to DCs both in vitro and in vivo. Vaccination with EXO-sensitized DCs significantly enhanced immune activation and inhibited tumor growth in the mouse HCC model compared with treatment using DCs alone.

MATERIALS AND METHODS

Mice

C57BL/6 wild type female mice (6-8 weeks of age) were used in all experiments. A subcutaneous tumor model was established, with three mice per group, and all experiments were independently repeated three times. All animal procedures were conducted in the animal facility of the University of Science and Technology of China and were reviewed and approved by the institutional ethics committee. Mice were euthanized at predefined endpoints by a CO_2 inhalation or cervical dislocation.

Cell Lines

The murine cell lines Hepa1-6 and DC2.4 were obtained from the Shanghai Cell Bank of the Chinese Academy of Sciences. Cells were cultured in DMEM (Hyclone, USA) supplemented with 10% fetal bovine serum (FBS), 100 U/mL penicillin, and 100 μg/mL streptomycin (Beyotime Biotechnology, China). Hepa1-6 cells were cultured in high-glucose DMEM, whereas DC2.4 cells were maintained in low-glucose DMEM to help maintain a less differentiated state. To eliminate exogenous exosomes, FBS was ultracentrifuged (Beckman

Optima XE-100, 120,000 ×g, for 14h) and filtered through 0.22 μm filter before us. All cells were cultured at 37°C in a humidified atmosphere containing 5% CO_2, with medium changes every 1-2 days and passaging during the logarithmic growth phase.

Preparation of Exosomes

Hepa 1-6 cells were cultured in exosome-depleted FBS during the logarithmic growth phase. After 48-hour of incubation, the conditioned medium was collected and centrifuged at 3,000×g for 15 min to remove cell debris and dead cells. The clarified supernatant was then mixed with exosome extraction reagent (SBI, USA) at a ratio of 5:1 (supernatant:reagent) and incubated at 4℃ overnight. The mixture was centrifuged at 1,500 ×g for 30 min at 4°C after which the supernatant was discarded. The resulting pellet was washed with PBS and centrifuged again under the same conditions (1,500 ×g, 5 min, at 4°C). The final exosome pellet was resuspended in PBS, and the protein concentration was quantified using a bicinchoninic acid (BCA) assay.

Transmission Electron Microscopy

Exosome morphology was examined using transmission electron microscopy (TEM). Briefly, 30 μL of the exosome suspension was applied to a piece of sealing film, and copper grids were immersed in the sample for 5 minutes. Excess liquid was removed by gentle blotting, and the grids were air-dried for approximately 10 minutes. The grids were then indirectly rinsed with PBS to remove unbound material, followed by staining with 30 μL of uranyl acetate for about 3 minutes. After a second PBS rinse and air-drying, the grids were allowed to stand for at least 30 minutes prior to TEM observation. This procedure enabled visualization of the exosomes' characteristic morphology and size.

Flow Cytometric Characterization of Cell Lines and Lymphocytes

DC2.4 cells were divided into treatment groups and exposed to PBS, EXOs (20 μg/mL), or LPS (1 μg/mL) for 48h in 12-well plates. After incubation, adherent cells from each group were collected, centrifuged, and washed for three times with precooled PBS at 4℃. Cell density was adjusted to 1×10^7cells/ml and blocked with PBS containing 10% rat serum at 4℃ for 15 min in the dark. Cells were then stained on ice for 30 minutes with fluorescently labeled antibodies against mouse CD86 (clone: GL-1, FITC), CD80 (clone: 16-10A1, PerCP/Cy5.5), CD83 (clone: Michel-19, PE), CD40 (clone: 3/23, APC), and MHC-II (clone: M5/114.15.2, Brilliant Violet 650), all from BioLegend, USA. DAPI (4 ‘, 6-diamino-2-phenylindole) was added to each tube prior to analysis, and the expression of cell surface markers was assessed by flow cytometry.

T-cell Proliferation Assay

Spleens from healthy C57BL/6 mice was harvested to prepare single-cell suspensions, followed by red blood cell lysis. T lymphocytes were isolated using magnetic beads and subsequently labeled with carboxyfluorescein diacetate succinimidyl ester (CFSE). CFSE-labeled T cells were co-cultured with DCs or exosome-pulsed DCs (DC-exo) at a ratio of 5:1 for 5 days. To prevent DC proliferation, DCs were pretreated with 10 μg/ml mitomycin for 2 hours prior to co-culture. After incubation, T cells were stained with monoclonal antibodies against CD4 and CD8 at 4℃ for 30 min. T cell proliferation in each experimental group was analyzed by flow cytometry with proliferating lymphocytes identified by reduced CFSE fluorescence intensity

Western Blot Analysis

Protein samples were mixed with loading buffer and denatured by heating at 100°C for 5 min. The proteins were separated by 12% SDS-PAGE and transferred onto PVDF membranes using wet transfer under constant current. Membranes were blocked with 5% bovine serum albumin (BSA) for 1 h at 25°C and then incubated overnight at 4°C with

primary antibodies against CD63, TSG101, and cytochrome C (Abcam, USA), each diluted at 1:1000 in 5% BSA. After washing with TBST, membranes were incubated with the appropriate secondary antibodies diluted at 1:4000 in 5% BSA for 1h at room temperature. Protein bands were visualized using a chemiluminescence imaging system.

Electron Microscopy of Exosomes

Exosome samples were resuspended in PBS and applied to copper grids by incubating the grids in 20 µL of EXOs suspension at 25°C for 5 min. Excess sample was removed from the edge of grids using filter paper, followed by air-drying. The grids were washed with PBS to remove unbound material. Negative staining was performed by incubating the grids in 30 µL of uranyl acetate at 25°C for 3 min, after which excess stain was removed with filter paper. The grids were then washed three additional times with PBS, air-dried at room temperature for approximately 30 min, and subsequently examined using a transmission electron microscope.

Ectopic Hepatocellular Carcinoma Models in Mice

Ectopic hepatocellular carcinoma (HCC) models were established by subcutaneous inoculation of Hepa1-6 cells (5×10^6 cells per mouse) into C57BL/6 mice. For standardized monitoring, tumor cells suspended in PBS were injected subcutaneously into the right flank region using a syringe under isoflurane anesthesia. Tumor growth was assessed every two days by measuring the length (L) and width (W) with calipers, and volume was calculated using the formula $(L\times W^2)/2$. Tumors were harvested when they reached an approximate volume of 1,000 mm^3. At the experimental endpoint, mice were euthanized and subcutaneous tumors exceeding 1 cm in diameter were excised, washed in D-Hanks' buffer, and digested with collagenase IV (1 mg/mL) and DNase I (50 µg/mL), all purchased from Gibco (Thermo Fisher Scientific, USA). After removal of necrotic tissues, tumors were minced into ~1 mm^3 fragments and mechanically dissociated DMEM. The resulting cell suspensions were filtered through 200-mesh gauze to obtain single-cell suspension, which were cultured for 3-5 passages. Cells were then collected and reinoculated subcutaneously (3×10^6 cells per mouse) into the axillary region of new recipient mice to establish a stable subcutaneous liver cancer model.

Measurement of T Lymphocytes in Murine Serum, Lymph Nodes, and Tumors

Peripheral blood samples were collected from treated HCC-bearing mice (DC-exo, DCs, or PBS groups) into tubes containing 1% heparin. Lymphocyte suspensions were prepared by lysing red blood cells at room temperature for 5 minutes. Isolated lymphocytes were stained for 1 hour at 4°C with a fluorescent antibody panel consisting of anti-mouse CD45 (clone: AP7), anti-mouse CD3 (clone: 17A2, Brilliant Violet 605), anti-mouse CD8 (clone: 53-6.7, PE), and anti-mouse CD4 (clone: RM4-5, FITC), followed by analysis by flow cytometry. For lymph node analysis, the skin over the hind limbs was carefully dissected to expose the inguinal lymph nodes, which were excised, washed twice with PBS, and processed into single-cell suspensions. Cells were stained with the same antibody panel used for blood samples. Tumor-infiltrating lymphocytes were isolated from excised tumor tissues. Tumors were minced into small fragments using surgical scissors and enzymatically digested in medium containing collagenase IV (2 mg/mL) and DNase I (100 µg/mL) for 1 hour at 37°C. The digested tissues was mechanically dissociated by pressing through a 200 µm steel mesh. After centrifugation at 800 ×g for 10 min, the pellets were resuspended in 5 mL of 40% Percoll, overlaid carefully with 2 ml of 70% percoll and centrifuged at 1260 ×g for 30 min at room temperature. Mononuclear cells at the interface were collected, washed twice with PBS, and stained with the antibody cocktail described above for flow cytometric analysis.

Statistical Methods

All statistical analyses and graphical representations were performed using GraphPad Prism 6.0. Data are presented as the mean±standard deviation (SD). Differences between two groups were analyzed using Student's t-test, while comparisons among multiple groups were performed using analysis of variance (ANOVA) followed by appropriate post hoc tests. A p value <0.05 was considered statistically significant.

RESULTS

Characteristics of Texs

Transmission electron microscopy (TEM) revealed that vesicles isolated from the Hepa 1-6 cell culture supernatant displayed a typical exosomal morphology, characterized by spherical or near-spherical, bilayer membrane structures with diameters ranging from approximately 30 to120 nm. The vesicles exhibited a relatively uniform size distribution and appearance at ×40,000 magnification, consistent with the morphological features of EXOs reported in the literature (Fig. 1A). Western blot analysis demonstrated the presence of the exosomal marker proteins CD63 and TSG101 were expressed in the Hepa 1-6–derived vesicle preparations, while cytochrome C was not detected. The findings indicate minimal contamination with cellular components or apoptotic debris and confirm the high purity the isolated EXOs (Fig. 1B and 1D). Nanoparticle tracking analysis (NTA) was used to assess the size of the isolated exosomes. Prior to analysis, exosome samples were appropriately diluted in 1× PBS, confirming a size range consistent with exosomes (Fig. 1C).

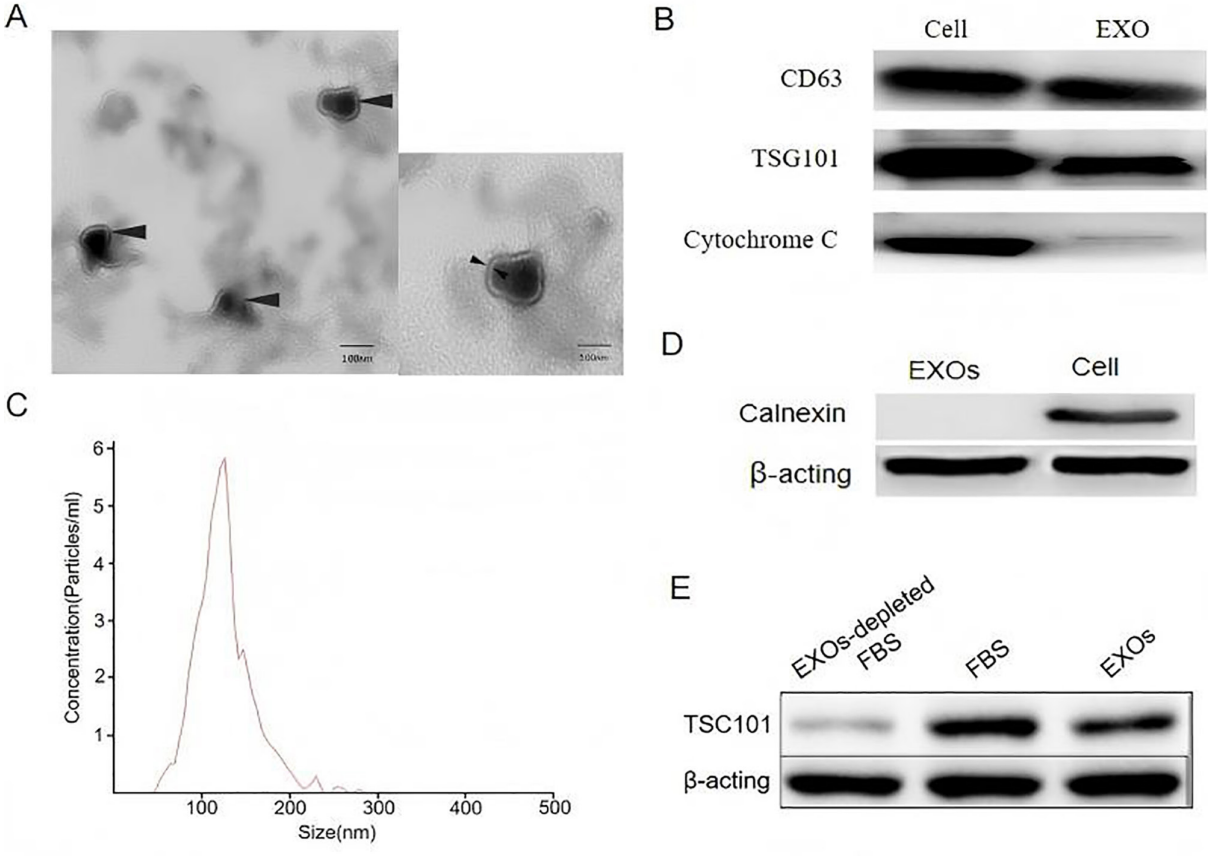

Fig. 1. (A) Transmission electron microscopy of hepa1-6–derived exosomes showing typical cup-shaped morphology. Scale bar represents 100 nm. (B) Western blot analyses of exosomal markers CD63 and TSG101 in isolated Hepa1-6 exosomes. (C) Particle size distribution of isolated exosomes determined by nanoparticle tracking analysis. (D) Western blot showing the absence of calnexin in isolated extracellular vesicles (EXOs), indicating minimal cellular contamination. (E) TSC101 expression is enriched in exosome-containing conditions.

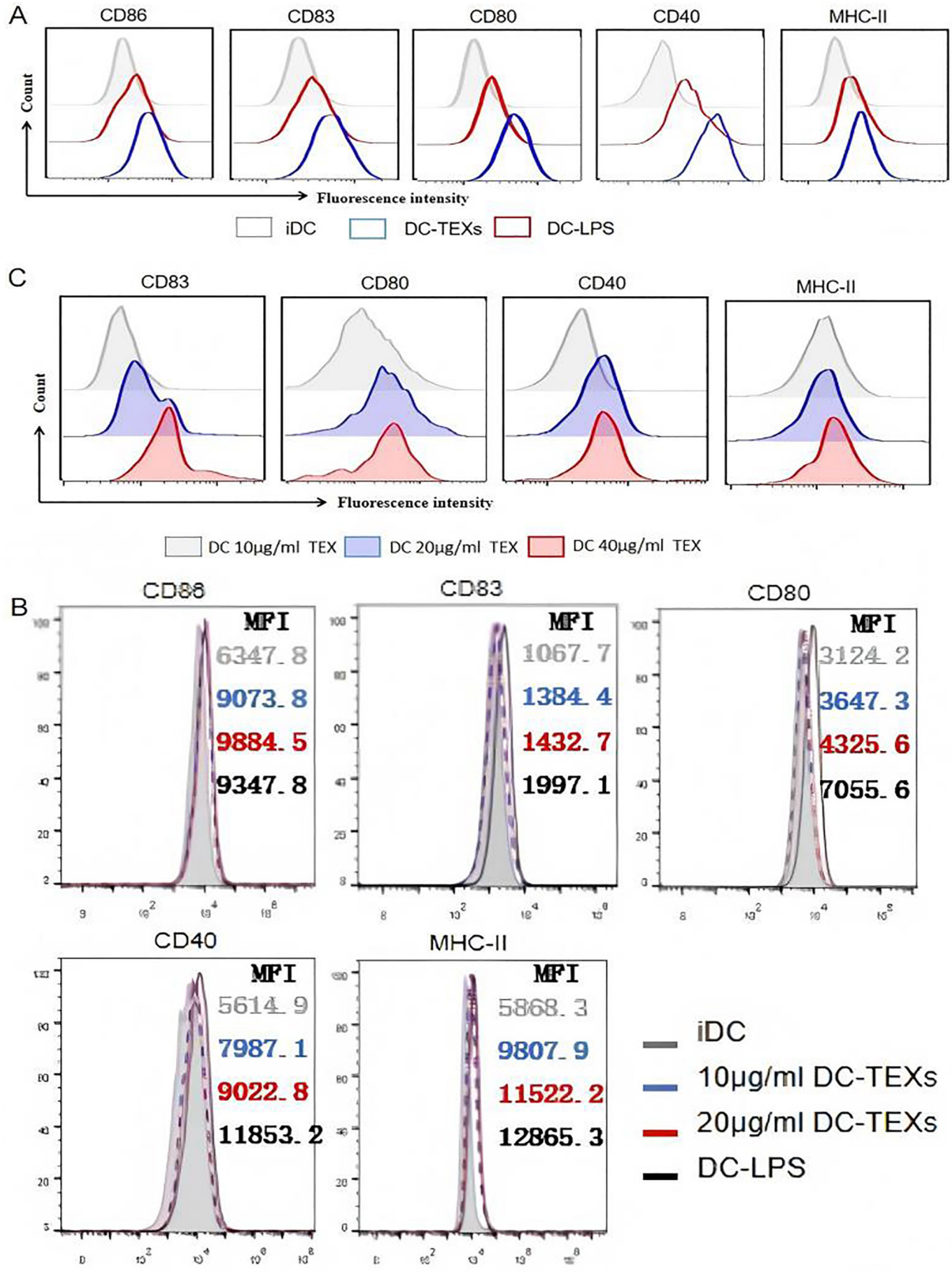

Fig. 2. (A) Flow cytometry analysis of surface molecule expression in immature DCs (iDCs), DCs pulsed with TEXs (DC-TEX) and LPS-treated DCs (DC-LPS). Expression of MHC-II，CD40, CD86, CD80 and CD83 was evaluated. CD40, APC-A; CD86, FITC-A; CD83, PE-A; CD80, PerCP Cy5.5-A; MHC-II, BV650-A. Lower panel shows mean fluorescence intensity (MFI)±standard error from three independent replicates. *P<0.05. (B) Quantification of MFI for MHC-II, CD40, CD86, CD80, and CD83 across experimental groups. *P<0.05. (C) Flow cytometry assessment of surface molecule expression in bone marrow–derived dendritic cells (BMDC). *P<0.05.

In addition, Western blotting showed the presence of TSG101 in untreated FBS and cell lysates but not in ultracentrifuged FBS, confirming the effective depletion of exosomes from the serum used for cell culture (Fig. 1E).

TEXs Induce DC-mediated Antitumor Immunity in vitro

After 48h of co-culture with Hepa 1-6-derived exosomes, DCs exhibited indicative of maturation, including increased cell volume, and partial suspension growth, and the appearance dendritic or pseudopod-like protrusions at the cell periphery. Flow cytometry analysis showed that, compared with the control group, the exosome treatment significantly upregulated the expression of DC maturation–associated surface molecules, including CD40, CD80, CD83, CD86 and MHC class II (Fig. 2A and 2B). Furthermore, the expression levels of these surface markers increased in a concentration-dependent manner with rising exosome doses (Fig. 2C). Flow cytometry confirmed a T-lymphocyte purity of 95.03% following magnetic bead isolation (Fig. 3A). Functional assays demonstrated that exosome-pulsed mature DCs induced significantly greater proliferation of naïve T cells compared with immature DCs ($P < 0.017$, Fig. 3B and 3C).

TEXs Induce DC-Mediated Antitumor Immunity in vivo

To evaluate TEX-induced, DC-mediated antitumor immune responses in vivo, a stable ectopic HCC mouse model was established (Fig. 4A). DCs were pulsed with an optimal dose of TEX (20 μg/mL) and compared with non-pulsed immature DCs.

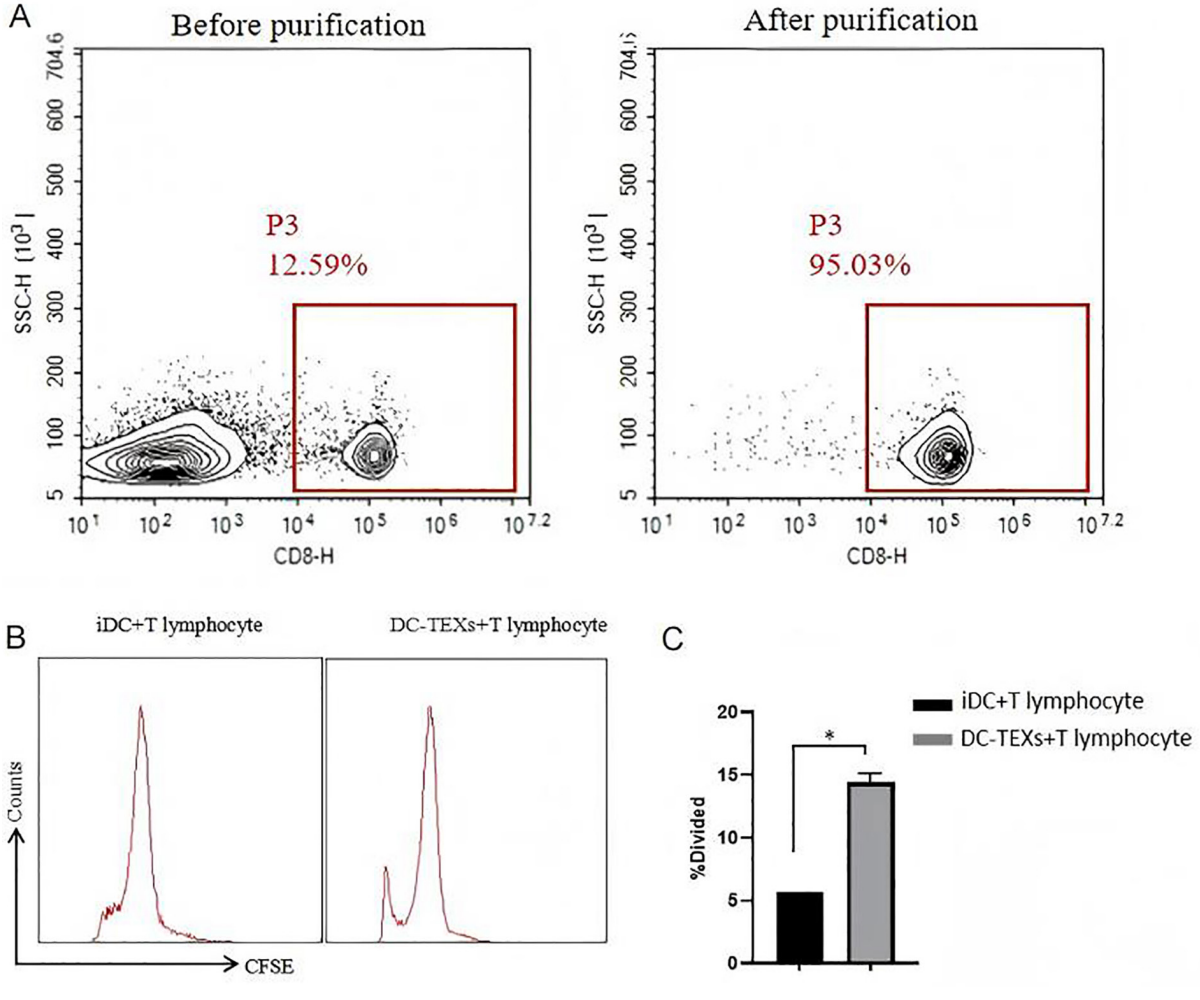

Fig. 3. (A) Purity of T cell populations after magnetic bead isolation, analyzed by flow cytometry. *P<0.05. (B, C) Proliferation of T lymphocytes induced in vitro by immature DCs (iDCs) and TEX-pulsed DCs (DC-TEX), assessed by flow cytometry. *P<0.05.

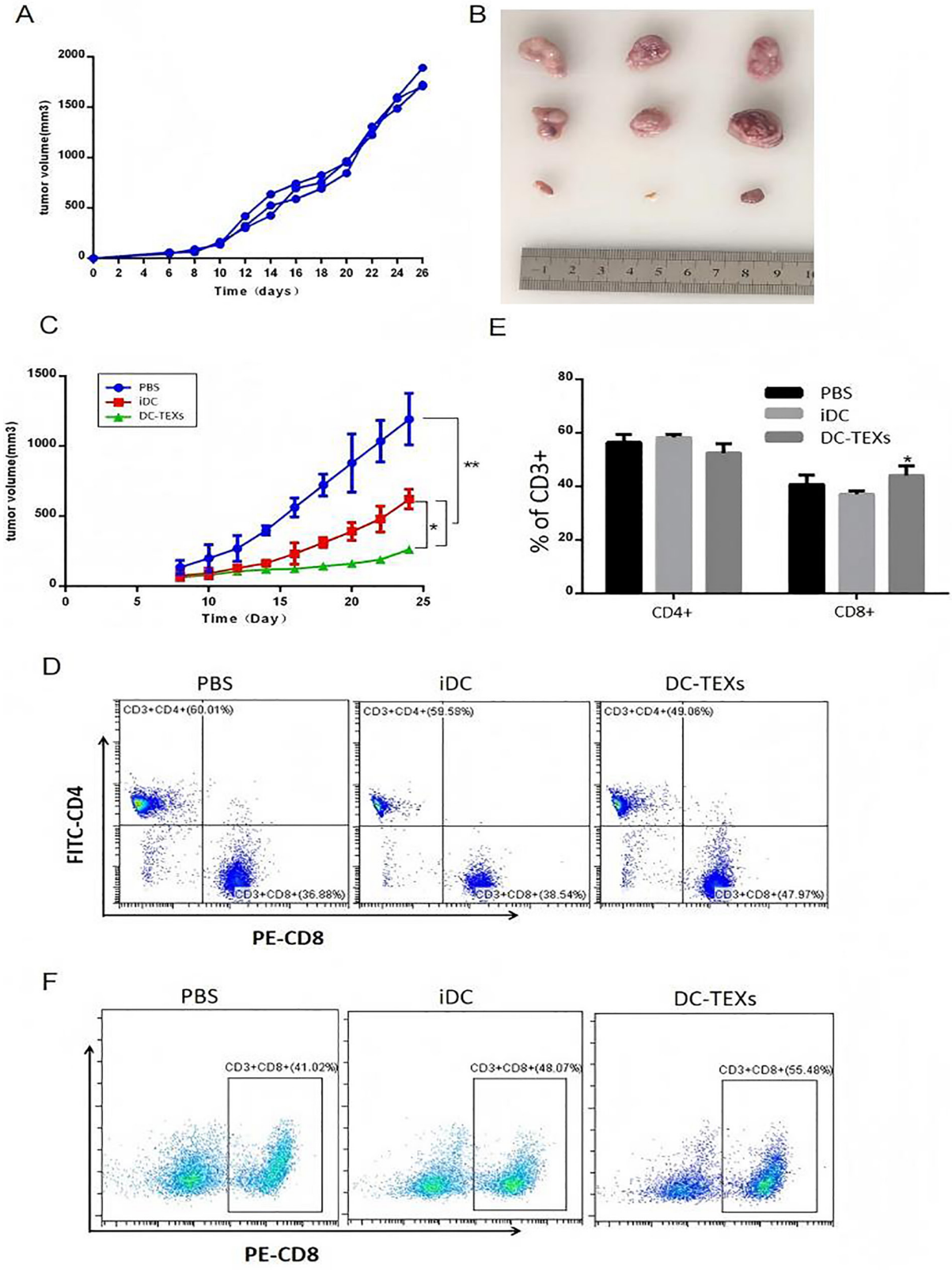

Fig. 4. (A) Line graph demonstrating the stability of the established ectopic hepatocellular carcinoma mouse model. (B) Representative images of resected tumors from C57BL/6 mice treated with DC-TEXs, iDCs, or PBS. (C) Tumor growth curves showing significant suppression in the DC-TEX group compared to the iDC and PBS groups by day 25 (two-tailed t-test, *P<0.05, n=3). (D-F) Flow cytometric analysis of $CD4^+$ and $CD8^+$ T lymphocytes in peripheral blood (D), lymph nodes (E), and tumor tissues (F) of tumor-bearing mice following treatment with DC-TEXs, iDCs, or PBS. DC-TEX treatment significantly increased $CD8^+$ T cell infiltration compared with the iDC group (two-tailed t-test, *P<0.05, n=3).

MHC-matched C57BL/6 mice bearing heterotopic tumors received weekly tail vein injections of DCs (3×10^6 cell per mouse) from the respective treatment groups for three consecutive weeks. Mice in the DC-TEX group exhibited markedly delayed tumor growth and significantly reduced tumor volumes compared with those in the iDC group (Fig. 4B and 4C). Furthermore, flow cytometric analysis revealed a significant increase in $CD8^+$ T lymphocytes in the peripheral blood (Fig. 4D), lymph nodes (Fig. 4E), and tumor tissues (Fig. 4F) of the DC–TEX group compared with the iDC and PBS groups. Mice in the DC–TEX group exhibited markedly delayed tumor growth and significantly reduced tumor volumes compared with those in the iDC group (Fig. 4B and 4C). In addition, flow cytometric analysis revealed a significant increase in $CD8^+$ T lymphocytes in the peripheral blood (Fig. 4D), lymph nodes (Fig. 4E), and tumor tissues (Fig. 4F) of the DC–TEX group compared with both the iDC and PBS control groups. Notably, the increase in lymph node T cell infiltration was specific to $CD8^+$ T cells, as no significant differences in $CD4^+$ T cell numbers were observed among the groups (Fig. 4E). These experiments were independently repeated three times with consistent results, indicating that DC pulsed with TEXs play a critical role in initiating cytotoxic T lymphocyte–mediated antitumor immune responses in vivo.

DISCUSSION

HCC remains a major clinical challenge, as most patients present with underlying chronic liver disease that promotes persistent immunosuppression (18). This pathological condition facilitates tumor progression and contributes to the establishment of an immunosuppressive tumor microenvironment that limits the effectiveness of immunotherapeutic strategies. Although DC-based immunotherapy has shown preliminary efficacy in clinical trials, its overall therapeutic benefit is often limited by insufficient T cell priming and the profoundly immunosuppressive milieu characteristic of HCC t (19-21). These limitations have prompted extensive research aimed at enhancing DC function, given their central role in initiating antigen-specific antitumor immunity through antigen processing, peptide-MHC complex presentation, and activation of naïve T cells (22). A key focus of these efforts is the identification of highly immunogenic tumor-derived antigens that can efficiently prime DCs while avoiding further exacerbation of the immunosuppressive tumor microenvironment. TEXs display dual immunomodulatory properties, with evidence indicating their ability to either enhance or suppress antitumor immune responses. In melanoma and breast cancer models, TEXs have been shown to transfer tumor-associated antigens (TAAs) and MHC molecules to DCs, thereby promoting DC activation and subsequent T-cell responses (23, 24). In contrast, other studies report that TEXs can exert immunosuppressive effects by delivering TGF-β, PD-L1, or specific miRNAs, which impair DC maturation and antigen presentation (25-27). These contrasting outcomes underscore the context-dependent nature of TEX-DC interactions, which are influenced by tumor cell origin, exosomal cargo composition, and disease stage, presenting challenges for the development of broadly applicable TEX-based immunotherapies.

Our study provides novel insights by demonstrating that Hepa 1-6-derived TEXs exert immunostimulatory effects on DCs. In vitro, TEX exposure induced concentration-dependent DC maturation, evidenced by upregulated expression of CD80, CD86, and MHC-II, which correlated with enhanced T cell proliferation. Mechanistically, proteomic analyses suggest that Hepa 1-6 TEXs carry multiple immunostimulatory components, including heat shock proteins (HSPs) and damage-associated molecular patterns

(DAMPs) (28, 29), which are known to engage TLRs and promote DC maturation. Additionally, the presence of MHC class I-peptide complexes in these TEXs, consistent with observations in other malignancies, may facilitate DC-mediated cross-presentation and amplify CD8+ T cell responses (30). In vivo, TEX-primed DCs induced significant tumor regression in subcutaneous HCC models, accompanied by increased infiltration of CD8+T cell without notable changes in CD4+T cell frequencies. This selective activation of CD8+T cell likely reflects the predominance of MHC class I–restricted antigens in Hepa 1-6 TEXs, as observed in other exosomal studies (31). Unlike DC vaccines pulsed with whole tumor lysates, which typically stimulate both CD4+ and CD8+ T cells, TEXs appear to preferentially promote cytotoxic T cell responses via cross-presentation (32). Nonetheless, the potential for CD4+T cell suppression by TEX-associated components such as indoleamine 2, 3-dioxygenase (IDO) or regulatory cytokines (33), warrants further investigation.

The partial tumor regression observed underscores the challenges posed by the immunosuppressive microenvironment of HCC, reflecting clinical experiences in which DC-based therapies rarely achieve complete responses in advanced disease. Persistent immunosuppressive factors, including regulatory T cells (Tregs), myeloid-derived suppressor cells (MDSCs), and immune checkpoint molecules, as well as variations in DC-TEX administration protocols, likely contribute to this limitation (34). Persistent immunosuppressive factors, including regulatory T cells (Tregs), myeloid-derived suppressor cells (MDSCs), and immune checkpoint molecules, as well as variations in DC–TEX administration protocols, likely contribute to this limitation (34). Key unresolved questions include: (1) identifying the specific TEX components (e.g., HSPs, DAMPs, nucleic acids, etc.) responsible for DC activation; (2) elucidating the mechanisms underlying CD4+ T cell unresponsiveness, given the critical role of CD4+ T cell help in sustaining long-term immune memory, potential strategies may involve engineering TEXs to incorporate MHC class II epitopes or Th1-polarizing cytokines; and (3) validating translational relevance using patient-derived HCC exosomes and human DCs to address possible species-specific differences in exosomal cargo and immune recognition. In conclusion, our findings demonstrate that Hepa 1-6-derived TEXs can effectively prime DCs to elicit antitumor immunity in HCC, highlighting their potential as antigen sources for DC-based immunotherapies. By evaluating both the immunostimulatory properties and immunosuppressive risks of TEXs, we provide a framework for optimizing TEX-DC strategies. Future studies should focus on detailed characterization of exosomal cargo, development of combination therapies, and optimization of delivery methods to overcome current limitations and facilitate the translation of TEX-based DC vaccines into clinical applications for HCC.

CONCLUSIONS

In summary, our study demonstrates that Hepa 1-6-derived exosomes effectively deliver HCC antigens and activate DC-mediated antitumor immunity in murine models, providing proof-of-concept for EXO-based DC immunotherapy and identifying a potential antigen repertoire for vaccine development. To advance this platform toward clinical translation, future studies should validate these findings in immunocompetent orthotopic HCC models that more accurately recapitulate human disease, and mechanistically investigate the interactions between EXO-primed DCs and tumor-infiltrating lymphocytes, with particular attention to immune checkpoint pathways (e.g., PD-1/PD-L1) that may limit therapeutic efficacy. Given the established role of DC dysfunction in tumor immune evasion, combining this approach with checkpoint

inhibitors or other immunomodulatory agents represents a promising strategy to counteract T cell exhaustion and enhance antitumor responses. These coordinated efforts will not only refine our understanding of EXO-mediated antigen presentation but may ultimately enable development of effective combinatorial immunotherapies for HCC.

CONFLICT OF INTEREST

The authors declare no conflicts of interests.

REFERENCES

1. Roberts SK, Majeed A, Rasaratnam K, Olynyk JK, Shackel N, Wood M, et al. National Survey of Real-World Australian Treatment Patterns for Patients With Very-Early-To Intermediate-Stage Hepatocellular Carcinoma. Cancer Med. 2025 Mar.14(5).
2. Zhao H, Mao Y, Wang H, Zhou A, Yang Z, Han Y, et al. A Survey of Clinical Practices for Hepatocellular Carcinoma Among Experts at Tertiary Hospitals in China From 2020 to 2021. Cancer Innov. 2025 Apr 7;4(3).
3. Afzal A, Abbasi MH, Ahmad S, Sheikh N, Khawar MB. Current Trends in Messenger RNA Technology for Cancer Therapeutics. Biomater Res. 2025 Apr 9;29:0178.
4. Llovet JM, Kelley RK, Villanueva A, Singal AG, Pikarsky E, Roayaie S, et al. Hepatocellular carcinoma. Nat Rev Dis Primers. 2021 Jan 21;7(1):6.
5. Villanueva A. Hepatocellular Carcinoma. N Engl J Med. 2019 Apr 11;380(15):1450-1462.
6. Sangro B, Sarobe P, Hervás-Stubbs S, Melero I. Advances in immunotherapy for hepatocellular carcinoma. Nat Rev Gastroenterol Hepatol. 2021 Aug;18(8):525-543.
7. Ni L. Advances in Human Dendritic Cell-Based Immunotherapy Against Gastrointestinal Cancer. Front Immunol. 2022 May 10;13:887189.
8. Shen KY, Zhu Y, Xie SZ, Qin LX. Immunosuppressive tumor microenvironment and immunotherapy of hepatocellular carcinoma: current status and prospectives. J Hematol Oncol. 2024 Apr 29;17(1):25.
9. Yu P, Han Y, Meng L, Tian Y, Jin Z, Luo J, et al. Exosomes derived from pulmonary metastatic sites enhance osteosarcoma lung metastasis by transferring the miR-194/215 cluster targeting MARCKS. Acta Pharm Sin B. 2024 May;14(5):2039-2056.
10. Fotouhi A, Hosseini M, Aghebati-Maleki A, Soltani-Zangbar MS, Parsania S, Mardi A, et al. The Impact of Wharton's Jelly-derived Exosomes on the Production of Inflammatory Mediators from HIG-82 Synoviocytes. Iran J Immunol. 2024 Sep 22;21(3):243-254.
11. Raposo G, Stoorvogel W. Extracellular vesicles: exosomes, microvesicles, and friends. J Cell Biol. 2013 Feb 18;200(4):373-83.
12. Hayashi N, Doi H, Kurata Y, Kagawa H, Atobe Y, Funakoshi K, et al. Proteomic analysis of exosome-enriched fractions derived from cerebrospinal fluid of amyotrophic lateral sclerosis patients. Neurosci Res. 2020 Nov;160:43-49.
13. Tutanov O, Orlova E, Proskura K, Grigor'eva A, Yunusova N, Tsentalovich Y, et al. Proteomic Analysis of Blood Exosomes from Healthy Females and Breast Cancer Patients Reveals an Association between Different Exosomal Bioactivity on Non-tumorigenic Epithelial Cell and Breast Cancer Cell Migration in Vitro. Biomolecules. 2020 Mar 25;10(4):495.
14. Urabe F, Ochiya T, Egawa S. Re: A Prospective Adaptive Utility Trial to Validate Performance of a Novel Urine Exosome Gene Expression Assay to Predict High-grade Prostate Cancer in Patients with Prostate-specific Antigen 2-10ng/ml at Initial Biopsy. Eur Urol. 2019 Aug;76(2):254-255.
15. Qian J, Lu E, Xiang H, Ding P, Wang Z, Lin Z, et al. GelMA loaded with exosomes from human minor salivary gland organoids enhances wound healing by inducing macrophage polarization. J Nanobiotechnology. 2024 Sep 6;22(1):550.
16. Li M, Li S, Du C, Zhang Y, Li Y, Chu L, et al. Exosomes from different cells: Characteristics, modifications, and therapeutic applications. Eur J Med Chem. 2020 Dec 1;207:112784.
17. Wan Z, Gao X, Dong Y, Zhao Y, Chen X, Yang G, et al. Exosome-mediated cell-cell communication in tumor progression. Am J Cancer Res. 2018 Sep 1;8(9):1661-1673.
18. Santagata S, Rea G, Castaldo D, Napolitano M, Capiluongo A, D'Alterio C, et al. Hepatocellular carcinoma (HCC) tumor microenvironment is more suppressive than colorectal cancer liver metastasis (CRLM) tumor microenvironment. Hepatol Int. 2024 Apr;18(2):568-581.
19. Jeng LB, Liao LY, Shih FY, Teng CF. Dendritic-Cell-Vaccine-Based Immunotherapy for Hepatocellular Carcinoma: Clinical Trials and Recent Preclinical Studies. Cancers (Basel). 2022 Sep 8;14(18):4380.
20. Teng CF, Wang T, Wu TH, Lin JH, Shih FY, Shyu WC, et al. Combination therapy with dendritic cell vaccine and programmed death ligand 1 immune

checkpoint inhibitor for hepatocellular carcinoma in an orthotopic mouse model. Ther Adv Med Oncol. 2020 Jun 10;12:1758835920922034.
21. Zuo B, Zhang Y, Zhao K, Wu L, Qi H, Yang R, et al. Universal immunotherapeutic strategy for hepatocellular carcinoma with exosome vaccines that engage adaptive and innate immune responses. J Hematol Oncol. 2022 Apr 29;15(1):46.
22. Wilson KR, Liu H, Healey G, Vuong V, Ishido S, Herold MJ, et al. MARCH1-mediated ubiquitination of MHC II impacts the MHC I antigen presentation pathway. PLoS One. 2018 Jul 12;13(7):e0200540.
23. Chen G, Huang AC, Zhang W, Zhang G, Wu M, Xu W, et al. Exosomal PD-L1 contributes to immunosuppression and is associated with anti-PD-1 response. Nature. 2018 Aug;560(7718):382-386.
24. Safaei S, Fadaee M, Farzam OR, Yari A, Poursaei E, Aslan C, et al. Exploring the dynamic interplay between exosomes and the immune tumor microenvironment: implications for breast cancer progression and therapeutic strategies. Breast Cancer Res. 2024 Mar 29;26(1):57.
25. Chatterjee S, Chatterjee A, Jana S, Dey S, Roy H, Das MK, et al. Transforming growth factor beta orchestrates PD-L1 enrichment in tumor-derived exosomes and mediates CD8 T-cell dysfunction regulating early phosphorylation of TCR signalome in breast cancer. Carcinogenesis. 2021 Feb 11;42(1):38-47.
26. Chen G, Huang AC, Zhang W, Zhang G, Wu M, Xu W, et al. Exosomal PD-L1 contributes to immunosuppression and is associated with anti-PD-1 response. Nature. 2018 Aug;560(7718):382-386.
27. Haderk F, Schulz R, Iskar M, Cid LL, Worst T, Willmund KV, et al. Tumor-derived exosomes modulate PD-L1 expression in monocytes. Sci Immunol. 2017 Jul 28;2(13):eaah5509.
28. Reddy VS, Madala SK, Trinath J, Reddy GB. Extracellular small heat shock proteins: exosomal biogenesis and function. Cell Stress Chaperones. 2018 May;23(3):441-454.
29. Abu N, Rus Bakarurraini NAA, Nasir SN. Extracellular Vesicles and DAMPs in Cancer: A Mini-Review. Front Immunol. 2021 Oct 15;12:740548.
30. Hao Y, Chen P, Zhang X, Shao Y, Xu Y, Qian W. The effects of tumor-derived exosomes on T-cell function and efficacy of cancer immunotherapy. Immun Med. 2021;1:e1029.
31. Matsuda-Lennikov M, Ohigashi I, Takahama Y. Tissue-specific proteasomes in generation of MHC class I peptides and CD8+ T cells. Curr Opin Immunol. 2022 Aug;77:102217.
32. Kikete S, Chu X, Wang L, Bian Y. Endogenous and tumour-derived microRNAs regulate cross-presentation in dendritic cells and consequently cytotoxic T cell function. Cytotechnology. 2016 Dec;68(6):2223-2233.
33. Troyer RM, Ruby CE, Goodall CP, Yang L, Maier CS, Albarqi HA, et al. Exosomes from Osteosarcoma and normal osteoblast differ in proteomic cargo and immunomodulatory effects on T cells. Exp Cell Res. 2017;358(2):369-76.
34. Lu Z, Zuo B, Jing R, Gao X, Rao Q, Liu Z, et al. Dendritic cell-derived exosomes elicit tumor regression in autochthonous hepatocellular carcinoma mouse models. J Hepatol. 2017 Oct;67(4):739-748.